Accurate finite-difference micromagnetics of magnets including RKKY interaction: Analytical solution and comparison to standard micromagnetic codes

D. Suess ●,[1,2] S. Koraltan ●,[1] F. Slanovc ●,[1] F. Bruckner,[1] and C. Abert[1,2]

[1]*Faculty of Physics, University of Vienna, 1090 Vienna, Austria*
[2]*Platform MMM Mathematics–Magnetism–Materials, University of Vienna, 1090 Vienna, Austria*

Within this paper we show the importance of accurate implementations of the Ruderman-Kittel-Kasuya-Yosida (RKKY) interactions for antiferromagnetically coupled ferromagnetic layers with thicknesses exceeding the exchange length. In order to evaluate the performance of different implementations of RKKY interaction, we develop a benchmark problem by deriving the analytical formula for the saturation field of two infinitely thick magnetic layers that are antiparallelly coupled. This benchmark problem shows that state of the art implementations in commonly used finite-difference codes lead to errors of the saturation field that amount to more than 20% for mesh sizes of 2 nm which is well below the exchange length of the material. In order to improve the accuracy, we develop higher order cell-based and nodal-based finite-difference codes that significantly reduce the error compared to state of the art implementations. For the second order cell-based approach and first order nodal-based approach the error of the saturation field is reduced by about a factor of 10 (2% error) for the same mesh size of 2 nm.

I. INTRODUCTION

Magnetic thin films build the backbone of various applications ranging from magnetic recording [1] to magnetic sensors [2]. Magnetic tunnel magnetoresistance (TMR) and giant magnetoresistance (GMR) sensors rely on antiferromagnetic coupled films in the reference system of the magnetic sensing system. In addition to the application of synthetic antiferromagnets in sensors, magnetic hard disk devices exhibit antiferromagnetically coupled soft magnetic underlayers, to minimize the magnetic stray field. The coupling strength of these magnetic layers can be well tuned via Ruderman-Kittel-Kasuya-Yosida (RKKY) interactions as an indirect magnetic exchange coupling through the 3*d*, 4*d*, and 5*d* transition metals, such as Ru or Cr [3,4]. Other magnetic systems where antiferromagnetic coupling has to be described accurately are ferrimagnetic structures that may exhibit antiparallel coupling between the net magnetization of the ferrimagnet and an adjacent ferromagnetic layer [5].

Due to the importance of antiferromagnetic coupling, micromagnetic codes usually offer the possibility to describe RKKY interaction. Commonly this is achieved by scaling the bulk exchange interaction to represent the RKKY interaction [6,7].

The finite-difference method usually assumes a homogeneous magnetization in each simulation cell with the finite-difference sampling points chosen in the cell centers [6–9]. In contrast, finite-element micromagnetic codes discretize the magnetization with an affine basis function with the unknown coefficients of the magnetization at the node points of the finite-element mesh. In between these node points the magnetization is commonly linearly interpolated [10]. The RKKY interaction can be implemented by adding a surface energy to the total energy, taking into account the RKKY interaction energy.

In Sec. II the micromagnetic theory including the RKKY interaction is reviewed. It is shown that the RKKY interaction alters the boundary condition for the magnetization. In Sec. III two analytical test cases are presented. The first test case consists of infinitely thin antiferromagnetically coupled ferromagnetic layers. The second test case is the opposing limit of infinitely thick antiferromagnetically coupled ferromagnetic layers. As we show in this paper, commonly used finite-difference micromagnetic codes are able to accurately describe thin antiferromagnetic coupled layers. However, these codes introduce significant errors both in the equilibrium magnetization as well as in critical fields if domain walls or partial domain walls are formed across the RKKY interface. In order to reduce these errors, we derive higher order implementations of the RKKY interaction of cell-centered finite-difference codes. In Sec. IV the higher order cell-based implementations and the node-based implementation are reviewed and compared to the result of the analytical benchmark problems of Sec. III.

II. GENERAL MICROMAGNETIC DESCRIPTION OF MAGNETIC REGIONS COUPLED VIA RKKY INTERACTION

In the following, we derive the differential equation for the magnetization in equilibrium from the total energy of the magnet as shown in Fig. 1. Here we assume the magnetic region Ω_1 and Ω_2. Within the domains Ω_1 and Ω_2 the magnetization $\boldsymbol{m}_1(\mathbf{x})$ and $\boldsymbol{m}_2(\mathbf{x})$ are continuous functions in space. At the common interface $\partial\Omega_1 \cap \partial\Omega_2$ the magnetization $\boldsymbol{m}_1(\mathbf{x})$ is not equal to $\boldsymbol{m}_2(\mathbf{x})$ in general. At this interface we assume a RKKY interaction.

For the considered general domain we start from the total energy E_{tot} that includes the exchange energy E_{ex}, anisotropy
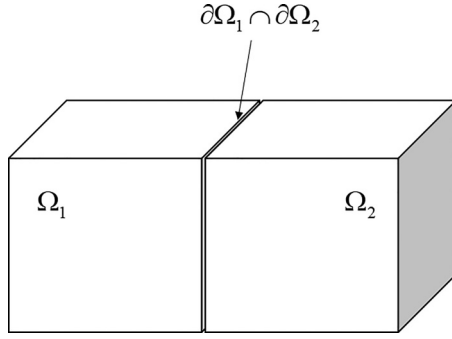
FIG. 1. Considered domain of a magnet with regions Ω_1 and Ω_2 that are coupled via the common interface $\partial\Omega_1 \cap \partial\Omega_2$.

energy E_{ani}, Zeeman energy E_{ext}, and RKKY surface interaction E_{rkky}:

$$E_{ani}(\mathbf{m}_1, \mathbf{m}_2) = -\int_{\Omega_1} K_{1,1}[\mathbf{m}_1 \cdot \mathbf{k}_1]^2 dV$$
$$-\int_{\Omega_2} K_{1,2}[\mathbf{m}_2 \cdot \mathbf{k}_2]^2 dV, \qquad (2.1)$$

$$E_{ext}(\mathbf{m}_1, \mathbf{m}_2) = -\int_{\Omega_1} J_{s,1}\mathbf{m}_1 \cdot \mathbf{H}_{ext} dV$$
$$-\int_{\Omega_2} J_{s,2}\mathbf{m}_2 \cdot \mathbf{H}_{ext} dV, \qquad (2.2)$$

$$E_{ex}(\mathbf{m}_1, \mathbf{m}_2) = \int_{\Omega_1} [A_{1,x}[\nabla m_{x,1}]^2 + A_{1,y}[\nabla m_{y,1}]^2$$
$$+ A_{1,z}[\nabla m_{z,1}]^2]dV$$
$$+ \int_{\Omega_2} [A_{2,x}[\nabla m_{x,2}]^2 + A_{2,y}[\nabla m_{y,2}]^2$$
$$+ A_{2,z}[\nabla m_{z,2}]^2]dV, \qquad (2.3)$$

$$E_{rkky}(\mathbf{m}_1, \mathbf{m}_2) = -\int_{\partial\Omega_1 \cap \partial\Omega_2} J_{rkky}\mathbf{m}_1 \cdot \mathbf{m}_2 dA. \qquad (2.4)$$

In these equations $K_{1,i}$ is the anisotropy constant in material i ($i = 1$ or 2); $\mathbf{k}_i$ the direction of the uniaxial easy axis; $J_{s,i}$ is the saturation magnetization; $A_{i,x}$, $A_{i,y}$, and $A_{i,z}$ are the exchange constants in the x, y, and z directions [11], respectively. $\mathbf{H}_{ext}$ is the external field and J_{rkky} the RKKY constant between the two materials.

The total energy is the sum of all energy terms:

$$E_{tot}(\mathbf{m}_1, \mathbf{m}_2) = E_{ex}(\mathbf{m}_1, \mathbf{m}_2) + E_{rkky}(\mathbf{m}_1, \mathbf{m}_2)$$
$$+ E_{ext}(\mathbf{m}_1, \mathbf{m}_2) + E_{ani}(\mathbf{m}_1, \mathbf{m}_2). \qquad (2.5)$$

Here, we ignore the stray-field energy, since the analytic benchmark problems that are constructed are without this long range interaction. The stray field does not change the boundary condition of the magnetization at interfaces.

The functional variation of the total energy according to Eq. (2.5) with respect to the magnetization $\mathbf{m}_1$ and $\mathbf{m}_2$ and the constraint $|\mathbf{m}_i| = 1$ is derived in detail in Appendix A. It leads to Brown's equation within the volumes Ω_i for the equilibrium magnetization $\mathbf{m}_i$:

$$\mathbf{m}_i \times [2\nabla \cdot (\mathbf{A}_i \nabla \mathbf{m}_i) + J_{s,i}\mathbf{H}_{ext} + 2K_{1,i}(\mathbf{m}_i \cdot \mathbf{k}_i)\mathbf{k}_i] = 0. \qquad (2.6)$$

For the interface to air, $\partial\Omega_1 \cup \partial\Omega_2 \backslash \partial\Omega_1 \cap \partial\Omega_2$, the well-known exchange boundary condition [12] applies:

$$(\nabla\mathbf{m}_i)\mathbf{n} = 0. \qquad (2.7)$$

Here, $\mathbf{n}$ is the normal vector at the boundary.

At the interface $\partial\Omega_1 \cap \partial\Omega_2$ where we assume RKKY interaction the following Robin boundary condition [13] is obtained:

$$2\mathbf{A}_1(\nabla\mathbf{m}_1)\mathbf{n} = -J_{rkky}(\mathbf{m}_1 \cdot \mathbf{m}_2)\mathbf{m}_1 + J_{rkky}\mathbf{m}_2. \qquad (2.8)$$

For Robin boundary conditions, the normal derivate of $\mathbf{m}_1$ is related to the value of $\mathbf{m}_1$ at the boundary. An equivalent boundary condition is obtained for the magnetization $\mathbf{m}_2$ for the common boundary $\partial\Omega_1 \cap \partial\Omega_2$.

For the case of $J_{rkky} = 0$ the boundary condition Eq. (2.8) reduces to the boundary condition of Eq. (2.7). For the case of $J_{rkky} = \infty$ it follows that $\mathbf{m}_1 = \mathbf{m}_2$ on $\partial\Omega_1 \cap \partial\Omega_2$. Hence, we obtain from Eq. (2.8) and the equivalent equation for the region Ω_2 the boundary condition between two magnets with different exchange constants [14]:

$$2\mathbf{A}_1(\nabla\mathbf{m}_1)\mathbf{n} - 2\mathbf{A}_2(\nabla\mathbf{m}_2)\mathbf{n} = 0. \qquad (2.9)$$

How a jump in the exchange constant can be correctly implemented in finite-difference micromagnetic codes is shown in Appendix C as well as with an alternative derivation in Ref. [9].

III. ANALYTIC SOLUTIONS FOR RKKY COUPLED LAYERS

A. Limit for thin layers—homogeneous magnetization within the layers

Here we consider the two antiparallelly coupled layers (i.e., $J_{rkky} < 0$) to be sufficiently thin so that the magnetization remains homogeneous within each layer. The thickness of each layer is t. The total energy for a system without anisotropy energy and demagnetizing energy is

$$E_{tot} = -J_{rkky}\int_F \mathbf{m}_1 \cdot \mathbf{m}_2 dA$$
$$- J_s\int_{\Omega_1} \mathbf{H} \cdot \mathbf{m}_1 dV - J_s\int_{\Omega_2} \mathbf{H} \cdot \mathbf{m}_2 dV. \qquad (3.1)$$

We obtain for the total energy E_{tot} divided by the surface area $F = \partial\Omega_1 \cap \partial\Omega_2$ between the two layers,

$$E_{tot}/F = -J_{rkky}\cos(2\varphi) - 2tJ_sH_x\cos(\varphi). \qquad (3.2)$$

Here the field is applied in the x direction and φ is the angle between the x axis and magnetization.

The equilibrium angle is obtained from the solution of

$$\frac{1}{2F}\frac{\partial E_{tot}}{\partial\varphi} = J_{rkky}\sin(2\varphi) + tJ_sH_x\sin(\varphi)$$
$$= J_{rkky}2\sin(\varphi)\cos(\varphi) + tJ_sH_x\sin(\varphi)$$
$$= 0, \qquad (3.3)$$

which leads to the nontrivial solution:

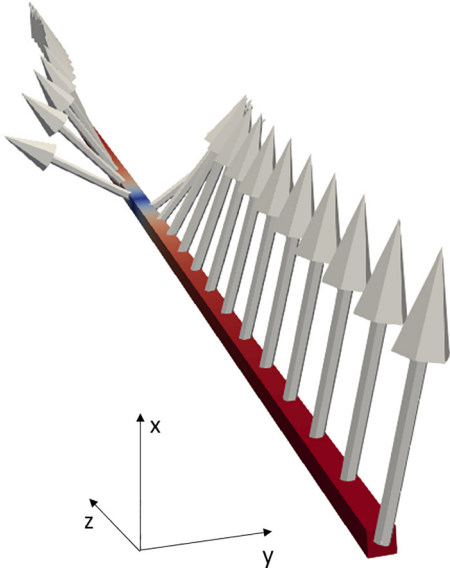$$\cos(\varphi) = m_{1,x} = -\frac{tJ_sH_x}{2J_{rkky}}. \qquad (3.4)$$

FIG. 2. Considered domain of the one-dimensional (1D) example. The region Ω_1 is from $-\infty < z \leqslant 0$ and Ω_2 is from $0 \leqslant z < \infty$. At the center at $z = 0$ the spins are antiferromagnetically coupled. Without external field the magnetization points parallel to the y axis which is parallel to the anisotropy axis. A field is applied in the $+x$ direction.

Obviously, the magnetization gets saturated for fields

$$H_{x,\text{sat}} = -\frac{2J_{\text{rkky}}}{tJ_s}. \tag{3.5}$$

B. Limit for infinitely thick layers—inhomogeneous magnetization within the layers

In order to test also RKKY implementations for the more complicated case, where inhomogeneous states are formed within the magnetic layers, we design a benchmark problem with an analytical solution. We consider an infinite one-dimensional (1D) magnet as shown in Fig. 2. At $z = 0$ the spins are coupled antiferromagnetically due to RKKY interaction. We assume the anisotropy direction $\mathbf{k} = (0, 1, 0)$ and $\mathbf{H}_{\text{ext}} = (H_x, 0, 0)$. As initial conditions we set the magnetization for $z > 0$ to $m_y = 1$ and for $z < 0$ to $m_y = -1$. For vanishing external field this initial configuration is a stable state. For increasing H_x the magnetization tends to align in the x direction while the anisotropy and RKKY interaction act against this alignment leading to inhomogeneous magnetization configurations within the ferromagnetic layers; see Fig. 2. Due to symmetry the magnetization for $z > 0$ can be written as

$$\mathbf{m}(z) = \begin{pmatrix} \cos[\varphi(z)] \\ \sin[\varphi(z)] \\ 0 \end{pmatrix}, \tag{3.6}$$

where $\varphi(z)$ is the angle between the x axis and the magnetization. At $z = 0$ the angle $\varphi(z)$ shows, in general, a jump and it holds as

$$\varphi(-z) = -\varphi(z). \tag{3.7}$$

As derived in Appendix B one obtains the relation between the angle $\varphi_0 = \varphi(z = 0)$ at one side of the RKKY interface
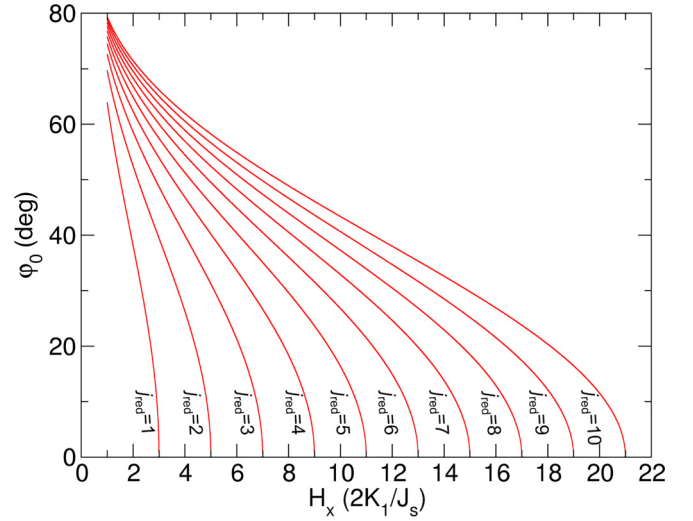

FIG. 3. Angle at the interface φ_0 as function of the external field H_x for different values of j_{red} obtained from the solution of Eq. (3.8).

and the applied field:

$$H_x = \frac{2K_1}{J_s} h_x = \frac{2K_1}{J_s} \frac{1}{4} \frac{\cos(2\varphi_0) - 1 - \overbrace{\frac{J_{\text{rkky}}^2}{2AK_1}}^{j_{\text{red}}} \sin^2(2\varphi_0)}{\cos(\varphi_0) - 1}. \tag{3.8}$$

Here, we introduced the dimensionless exchange and external field parameter:

$$j_{\text{red}} = \frac{J_{\text{rkky}}^2}{2AK_1}, \tag{3.9}$$

$$h_x = \frac{J_s H_x}{2K_1}. \tag{3.10}$$

The angle at the interface φ_0 as a function of the external field H_x for different values of j_{red} obtained from the solution of Eq. (3.8) is shown in Fig. 3.

After calculating the angle φ_0 for a particular field H_x, also the entire domain wall profile $\varphi(z)$ can be obtained using Eq. (B19). The analytic solution agrees very well with the finite-element solution of MAGNUM.FE as shown in Fig. 4. A discrepancy between the MUMAX3 [6] solution and the analytic solution can be seen in Fig. 4.

The critical field $h_{x,\text{sat}}$, where the entire structure is perfectly saturated, is derived in Appendix B as

$$H_{x,\text{sat}} = \frac{2K_1}{J_s} h_{x,\text{sat}} = \frac{2K_1}{J_s}\left(1 + \frac{J_{\text{rkky}}^2}{AK_1}\right). \tag{3.11}$$

In the following this saturation field will be used to test various micromagnetic RKKY implementations.

IV. FINITE-DIFFERENCE (FD) DISCRETIZATION OF RKKY INTERFACES

A. Cell-based FD approach

Here, we will show how RKKY interactions can be implemented in cell-based finite-difference codes. RKKY
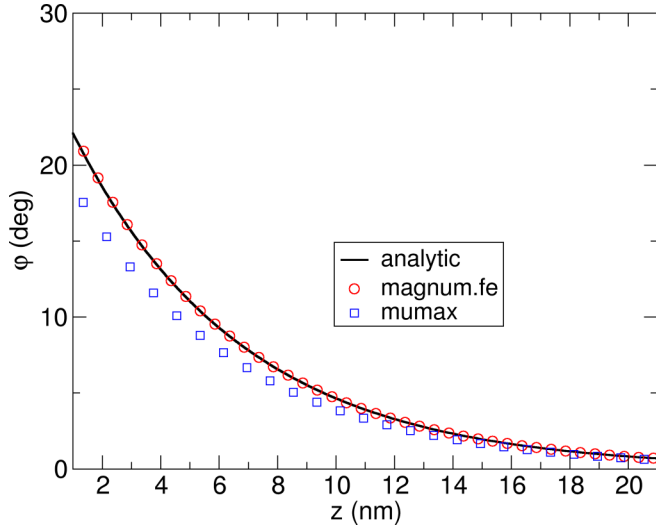
FIG. 4. Spin angle φ as a function of the z coordinate for $h_x = 4$, $j_{\text{red}} = 2$, and a mesh size of $\Delta z = 0.5$ nm for (MAGNUM.FE) finite-element code and (MUMAX3), a finite-difference code. The analytical solution is according to Eqs. (3.8) and (B19).

interactions might lead to antiparallel or weak coupling between these coupled layers [4,15]. In the following we will derive a zero, first, and second order method to treat these interactions.

We assume an infinitely thin spacer layer at $z = 0$ as shown in Fig. 5. The exchange field at the left side of the interface
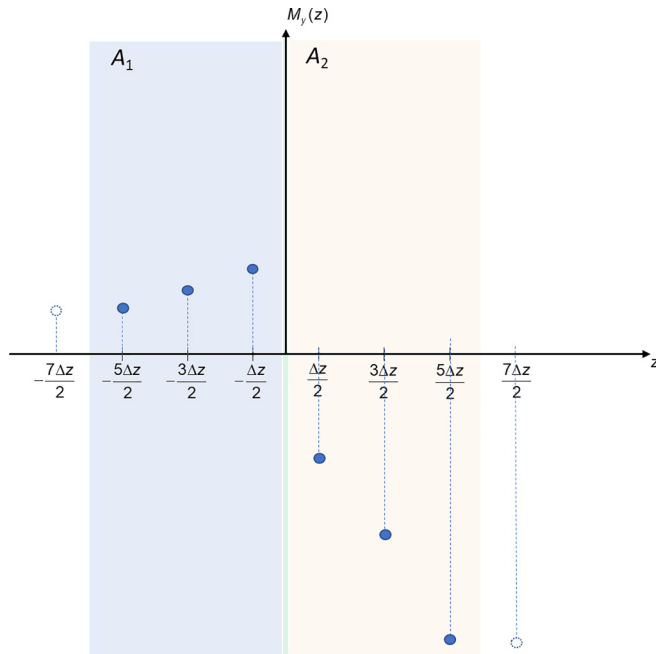

FIG. 5. Finite-difference discretization for cell-based finite-difference method. The discretization points for the magnetization are located at the cell centers. The spacer layer which couples the magnetization $\boldsymbol{m}(-\Delta z/2)$ and the magnetization $\boldsymbol{m}(\Delta z/2)$ is assumed to be infinitely thin. The thickness of the two magnets is, in this example, $3\Delta z$ each.

$(z = \Delta z/2)$ is given by Eq. (A14) as

$$\mathbf{H}_{\text{ex}}\left(-\frac{\Delta z}{2}\right) = \frac{2A}{J_s}\mathbf{m}''_1\left(-\frac{\Delta z}{2}\right), \quad (4.1)$$

where we approximate

$$\mathbf{m}''_1\left(-\frac{\Delta z}{2}\right) = \frac{\mathbf{m}'_1(0) - \mathbf{m}'_1(-\Delta z)}{\Delta z} + O(\Delta z^2), \quad (4.2)$$

with a truncation error $O(\Delta z^2)$.

The boundary condition at $z = 0$ is given by

$$\mathbf{m}'_1(0) = -\frac{J_{\text{rkky}}}{2A_1}[\mathbf{m}_1(0) \cdot \mathbf{m}_2(0)]\mathbf{m}_1(0) + \frac{J_{\text{rkky}}}{2A_1}\mathbf{m}_2(0). \quad (4.3)$$

Here it is important to note that it is relevant to consider the first term on the right-hand side of Eq. (4.3). If this term is neglected, significant deviations of the correct interpolation are obtained for the higher order methods. Only for the interpolation order $O(0)$ does this term cancel out and hence need not be considered.

One obtains the following:

$$\mathbf{H}_{\text{ex}}\left(-\frac{\Delta z}{2}\right)$$
$$= \frac{J_{\text{rkky}}\{\mathbf{m}_2(0) - [\mathbf{m}_1(0) \cdot \mathbf{m}_2(0)]\mathbf{m}_1(0)\} - 2A\mathbf{m}'_1(-\Delta z)}{J_s\Delta z}$$
$$+ O(\Delta z^2). \quad (4.4)$$

The second term on the right-hand side of Eq. (4.2) is simply obtained by a central finite-difference approximation with a truncation error $O(\Delta z^2)$:

$$\mathbf{m}'_1(-\Delta z) = \frac{\mathbf{m}_1\left(-\frac{\Delta z}{2}\right) - \mathbf{m}_1\left(-\frac{3\Delta z}{2}\right)}{\Delta z} + O(\Delta z^2). \quad (4.5)$$

For the evaluation of $\mathbf{m}_1(0)$ and $\mathbf{m}_2(0)$ different interpolation orders can be used:

Order (0). The magnetization in Ω_1 and Ω_2 is simply approximated as

$$\mathbf{m}_1(0) = \mathbf{m}_1\left(-\frac{\Delta z}{2}\right) + O(\Delta z), \quad (4.6)$$

$$\mathbf{m}_2(0) = \mathbf{m}_2\left(\frac{\Delta z}{2}\right) + O(\Delta z), \quad (4.7)$$

with truncation errors $O(\Delta z)$ that are linear in Δz.

By neglecting all terms parallel to $\mathbf{m}_1(-\frac{\Delta z}{2})$ [hence the second term on the right-hand side of Eq. (4.3) cancels out, which is a commonly used interpolation in O(0) codes] we get

$$\mathbf{H}_{\text{ex}}\left(-\frac{\Delta z}{2}\right) = \frac{1}{J_s\Delta z^2}\left[J_{\text{rkky}}\Delta z\mathbf{m}_2\left(\frac{\Delta z}{2}\right)\right.$$
$$\left. + 2A_1\mathbf{m}_1\left(-\frac{3\Delta z}{2}\right)\right]. \quad (4.8)$$

Order (1). We approximate the magnetization in Ω_1 and Ω_2 with a series expansion up to truncation errors of order

$$\mathbf{m}_1(0) = \mathbf{m}_1\left(-\frac{\Delta z}{2}\right) + \frac{\Delta z}{2}\mathbf{m}'_1\left(-\frac{\Delta z}{2}\right) + O(\Delta z^2). \quad (4.9)$$

Using the backward difference approximation [16,17] of the first derivative leads to

$$\mathbf{m}'_1\left(-\frac{\Delta z}{2}\right) = \frac{1}{\Delta z}\left[\mathbf{m}_1\left(-\frac{\Delta z}{2}\right) - \mathbf{m}_1\left(-\frac{3\Delta z}{2}\right)\right] + O(\Delta z),$$
(4.10)

$$\mathbf{m}_1(0) = \mathbf{m}_1\left(-\frac{\Delta z}{2}\right) + \frac{1}{2}\left[\mathbf{m}_1\left(-\frac{\Delta z}{2}\right) - \mathbf{m}_1\left(-\frac{3\Delta z}{2}\right)\right]$$
$$+ O(\Delta z^2).$$
(4.11)

This extrapolation and the extrapolation of $\mathbf{m}_2(0)$ that can be done in an analog fashion is used within Eq. (4.4) for the calculation of the effective field at the boundary cells.

Order (2). Increasing the interpolation order of the first and second derivatives using the backward difference approximation of $\mathbf{m}'_1(-\Delta z/2)$ and $\mathbf{m}''_1(-\Delta z/2)$ leads to

$$\mathbf{m}_1(0) = \mathbf{m}_1\left(-\frac{\Delta z}{2}\right) + \frac{\Delta z}{2}\mathbf{m}'_1\left(-\frac{\Delta z}{2}\right)$$
$$+ \frac{1}{2}\left(\frac{\Delta z}{2}\right)^2\mathbf{m}''_1\left(-\frac{\Delta z}{2}\right) + O(\Delta z^3).$$
(4.12)

Using the backward difference approximation [16,17] of the first derivative up to $O(\Delta z^2)$ and the second derivative up to $O(\Delta z)$, we obtain

$$\mathbf{m}'_1\left(-\frac{\Delta z}{2}\right) = \frac{1}{2\Delta z}\left[3\mathbf{m}_1\left(-\frac{\Delta z}{2}\right) - 4\mathbf{m}_1\left(-\frac{3\Delta z}{2}\right)\right.$$
$$\left. + \mathbf{m}_1\left(-\frac{5\Delta z}{2}\right)\right] + O(\Delta z^2),$$

$$\mathbf{m}''_1\left(-\frac{\Delta z}{2}\right) = \frac{1}{\Delta z^2}\left[\mathbf{m}_1\left(-\frac{\Delta z}{2}\right) - 2\mathbf{m}_1\left(-\frac{3\Delta z}{2}\right)\right.$$
$$\left. + \mathbf{m}_1\left(-\frac{5\Delta z}{2}\right)\right] + O(\Delta z),$$
(4.13)

leading to

$$\mathbf{m}_1(0) \approx \frac{15}{8}\mathbf{m}_1\left(-\frac{\Delta z}{2}\right) - \frac{5}{4}\mathbf{m}_1\left(-\frac{3\Delta z}{2}\right) + \frac{3}{8}\mathbf{m}_1\left(-\frac{5\Delta z}{2}\right)$$
$$+ O(\Delta z^3).$$
(4.14)

These zero, first, and second order interpolations can be found in the code used for this paper [18]; we also implemented it in the latest release of the finite-difference code MAGNUM.NP release [19]. For the interpolation of $\mathbf{m}'_1(-\Delta z/2)$ we evaluated the $O(\Delta z)$ implementation according to Eq. (4.5) as well as a higher order interpolation $O(\Delta z^2)$. For the investigated example the $O(\Delta z^2)$ interpolation of $\mathbf{m}'_1(-\Delta z/2)$ did not show considerable improvement of the results.

It is worth noting that for the cell-based finite-difference method the ghost cell has to be set on the left boundary as follows (an equivalent condition is used for the right boundary):

$$\mathbf{m}_{-7\Delta z/2} = \mathbf{m}_{-5\Delta z/2}.$$
(4.15)

If

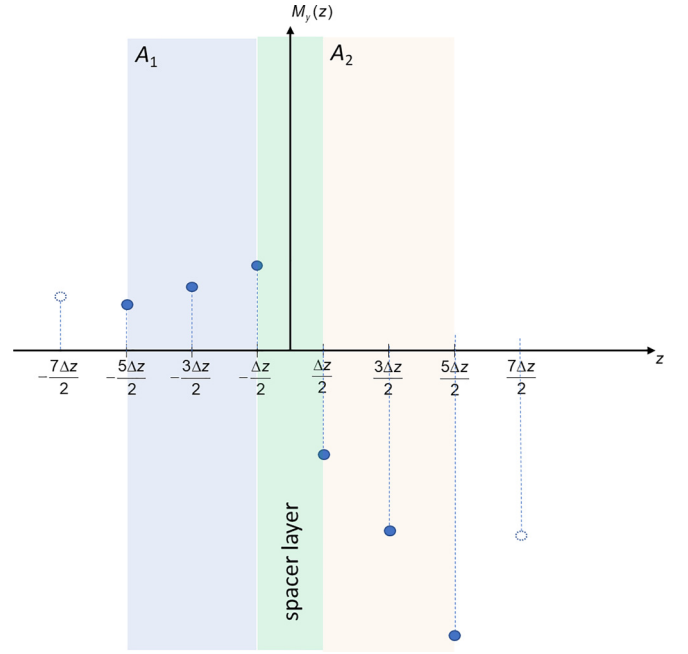$$\mathbf{m}_{-7\Delta z/2} = \mathbf{m}_{-3\Delta z/2}$$
(4.16)

FIG. 6. Finite-difference discretization for node-based finite-difference method. The magnetization is given on the mesh nodes. The spacer layer which couples the magnetization $m(-\Delta z/2)$ and the magnetization $m(\Delta z/2)$ has a thickness of Δz. The thickness of the two magnets is, in this example, $2\Delta z$ each.

is used as the boundary condition (as it is done for node-based finite-difference codes) a significant deviation of the results is obtained as shown in Fig. 7 (cell O1, low order BC), where BC stands for boundary condition.

B. Node-based FD approach

Since the inclusion of RKKY interactions is more naturally possible within a node-based finite-difference scheme, we also show this approach here.

We assume a spacer layer between the nodes at $z = -\Delta z/2$ and $z = \Delta z/2$ as shown in Fig. 6. The coupling between the nodes is given by Eq. (2.4) which leads to the boundary condition given by Eq. (2.8). In order to derive the exchange field at $z = -\Delta z/2$ we again start from

$$\mathbf{H}_{ex}\left(-\frac{\Delta z}{2}\right) = \frac{2A}{J_s}\mathbf{m}'_1\left(-\frac{\Delta z}{2}\right),$$
(4.17)

where we approximate

$$\mathbf{m}''_1\left(-\frac{\Delta z}{2}\right) = \frac{\mathbf{m}'_1\left(-\frac{\Delta z}{2}\right) - \mathbf{m}'_1(-\Delta z)}{\Delta z/2}.$$
(4.18)

From the boundary condition Eq. (2.8) at $z = -\Delta z/2$ follows by neglecting again all terms parallel to $\mathbf{m}_1(-\frac{\Delta z}{2})$ (since it does not change the dynamics of the system):

$$\mathbf{m}'_1\left(-\frac{\Delta z}{2}\right) = \frac{J_{rkky}}{2A_1}\mathbf{m}_2\left(\frac{\Delta z}{2}\right).$$
(4.19)

Hence,

$$\mathbf{H}_{ex}\left(-\frac{\Delta z}{2}\right) = \frac{2}{J_s\Delta z}\left[J_{rkky}\mathbf{m}_2\left(\frac{\Delta z}{2}\right) - 2A\mathbf{m}'_1(-\Delta z)\right].$$
(4.20)

The second term on the right-hand side of Eq. (4.20) is again obtained by a finite-difference approximation:

$$\mathbf{m}'_1(-\Delta z) = \frac{\mathbf{m}_1\left(-\frac{\Delta z}{2}\right) - \mathbf{m}_1\left(-\frac{3\Delta z}{2}\right)}{\Delta z}. \quad (4.21)$$

Hence, we obtain the following for the exchange field:

$$\mathbf{H}_{ex}\left(-\frac{\Delta z}{2}\right) = \frac{2}{J_s \Delta z^2}\left[J_{rkky}\Delta z \mathbf{m}_2\left(\frac{\Delta z}{2}\right)\right.$$
$$\left. + 2A_1 \mathbf{m}_1\left(-\frac{3\Delta z}{2}\right)\right]. \quad (4.22)$$

It is worth noting that this formula for the RKKY interface contains a term $4A_1$, whereas the formula within the bulk of the magnet contains a term of $2A$ as can be seen in Eq. (C14). In Appendix D it is shown that in one-dimensional (1D) systems the calculation of the effective field according to Eq. (4.22) is equivalent to a 1D finite-element implementation of RKKY interaction.

For this nodal-based finite-difference method, the ghost cell has to be set on the left boundary following the central difference approximation of Brown's boundary condition (an equivalent condition is used for the right boundary):

$$\mathbf{m}_{-7\Delta z/2} = \mathbf{m}_{-3\Delta z/2}. \quad (4.23)$$

If the one-sided finite difference

$$\mathbf{m}_{-7\Delta z/2} = \mathbf{m}_{-5\Delta z/2} \quad (4.24)$$

is used as the boundary condition a significant deviation of the results is obtained as shown in Fig. 7 (node, low order BC).

V. COMPARISON OF ANALYTICAL SOLUTION WITH MICROMAGNETIC SIMULATIONS

A. Limit for thin layers—homogeneous magnetization within the layers

All tested micromagnetic codes were able to accurately reproduce the hysteresis loop of two antiferromagnetic thin layers as shown in Fig. 7 (material parameters are listed in the caption of Fig. 7). Here, the stray field is not considered. This test case was primarily chosen to validate the different definitions of the exchange implementations of the codes, which correspond to

$$E_{rkky,OOMMF}(\mathbf{m}_1, \mathbf{m}_2) = -2\int_{\partial\Omega_1 \cap \partial\Omega_2} J_{rkky}\mathbf{m}_1 \cdot \mathbf{m}_2 dA, \quad (5.1)$$

$$E_{rkky,MUMAX}(\mathbf{m}_1, \mathbf{m}_2) = -\int_{\partial\Omega_1 \cap \partial\Omega_2} J_{rkky}\mathbf{m}_1 \cdot \mathbf{m}_2 dA. \quad (5.2)$$

It is interesting to note that the proper implementation of the Neumann boundary condition at the air surface is important for accurate results. Figure 7 (paper, node) shows the node-based RKKY implementation according to Eq. (4.22) and the correct boundary condition according to Eq. (4.23). Here perfect agreement with the analytic result (3.5) is observed. In contrast Fig. 7 (paper, node, low order BC) shows the same node-based RKKY implementation according to Eq. (4.22) but a different boundary condition according to
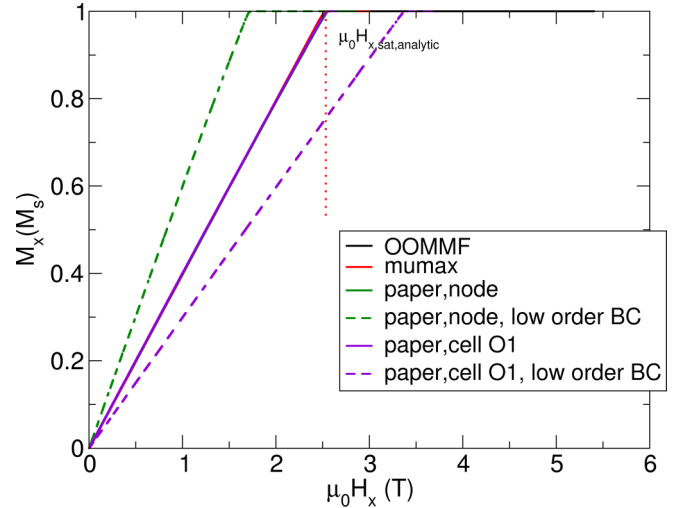

FIG. 7. Hysteresis loop of two antiferromagnetic coupled thin films, where each layer has a thickness of $t = 2$ nm, $A = 5 \times 10^{-11}$ J/m, $K_1 = 0$, $J_s = 1$ T. The analytic result is obtained from Eq. (3.5). Different finite-difference implementations are tested. (OOMMF) $J_{rkky,oommf} = -0.001$ J/m^2. (MUMAX3) Solution $J_{rkky,mumax} = -0.002$ J/m^2. (Paper, cell O1) Cell-based RKKY implementation according to Eq. (4.6) and boundary condition according to Eq. (4.15) and $J_{rkky,this paper} = -0.002$ J/m^2. (Paper, cell O1, low order BC) Cell-based RKKY implementation according to Eq. (4.6) and boundary condition according to (4.16). (Paper, node) Node-based RKKY implementation according to Eq. (4.22) and the boundary condition according to Eq. (4.23). (Paper, node, low order BC) Node-based RKKY implementation according to Eq. (4.22) and the boundary condition according to Eq. (4.24).

Eq. (4.24). Here, a significant error occurs. An equivalent situation can be observed with the cell-based implementation.

B. Limit for thick layers—inhomogeneous magnetization within the layers

The test cases for thin magnetic layers, where no partial domain walls arise within the magnetic layers can be well reproduced by all micromagnetic codes. The situation is different if inhomogeneous states are formed within the magnetic layers. To realize this situation we use the analytically derived benchmark problem of the saturation field according to Eq. (3.11).

In the following, we perform micromagnetic simulations for the parameters $A = 10^{-11}$ J/m, $K_1 = 10^5$ J/m^3, $J_s = 1$ T, and $J_{rkky} = -2 \times 10^{-3}$ J/m^2 using the finite-element code MAGNUM.FE [20] and different state of the art finite-difference codes (MUMAX and OOMMF) as well as different RKKY implementations according to this paper. The external field is slowly increased within 500 ns from $h_x = 3.5$ to $h_x = 5.5$, where h_x is the field in units of $2K_1/J_s$. The hysteresis loop close to the saturation field is shown in Fig. 8. Excellent agreement between the finite-element solution obtained by MAGNUM.FE and the analytic solution, which is $h_{x,crit} = 5$, can be obtained for various mesh sizes as shown in Fig. 9. The saturation field is evaluated by calculating the second derivative of the $M_x(H_x)$. The field where the second derivative has its minimum value is evaluated as the saturation field $H_{x,sat}$, since it describes the
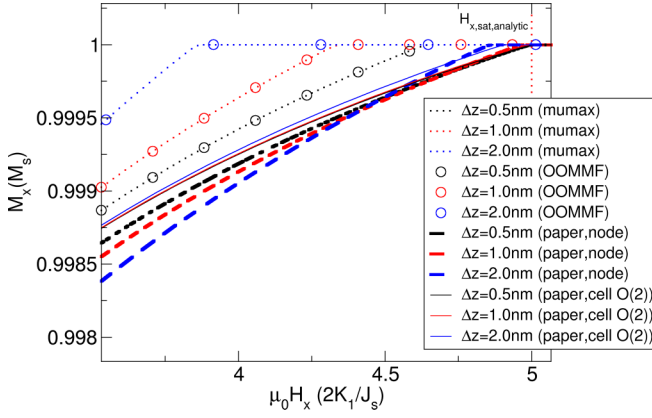
FIG. 8. (a) Micromagnetically obtained $M_x(H_x)$ loop for a structure with lateral dimensions $-400\,\text{nm} < z < 400\,\text{nm}$, $-1\,\text{nm} < x < 1\,\text{nm}$, $-1\,\text{nm} < y < 1\,\text{nm}$ for different mesh sizes Δz and different codes. (MUMAX) Finite-difference code with cell-centered magnetization. (OOMMF) Finite-difference code with the same interpolation as MUMAX. (Paper,node) nodal-based finite-difference code according to Eq. (4.22) for the RKKY interaction. (Paper, cell O2) cell-based finite-difference code according to Eq. (4.14) for the RKKY interaction. The analytically obtained saturation field is $H_{x,\text{sat,analytic}} = 5 \times 2K_1/J_s$.
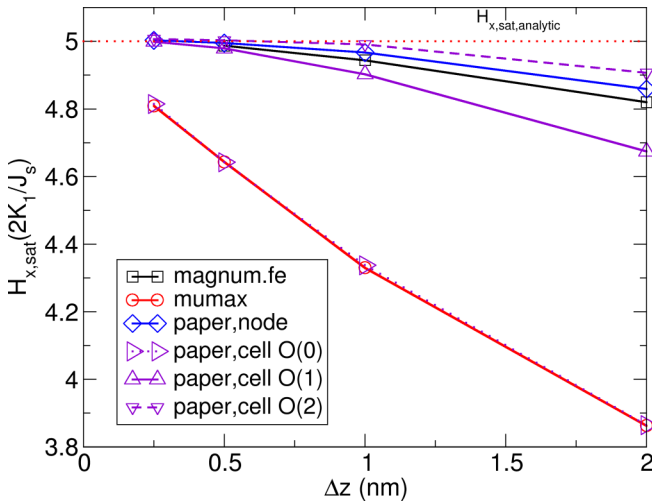

FIG. 9. Obtained saturation field $H_{x,\text{sat}}$ for the same example as Fig. 8 for different discretization lengths for different micromagnetic methods. (MUMAX) Only in the limit of infinitely small mesh size is good agreement with the analytic value obtained. MAGNUM.FE is a finite-element code with linear shape functions for the magnetization between the node points. The finite-element method shows a much better convergence. (Paper,node) The finite-difference implementation according to Eq. (4.22), which is equivalent to the finite-element 1D case, shows similarly good convergence. (Paper, cell O0) the cell-centered finite-difference method order zero of the interpolation of m_0 according to Eq. (4.8). (Paper, cell O1) the cell-centered finite-difference method of order 1 according Eq. (4.11). (Paper, cell O2) the cell-centered finite-difference method of order 2 according to Eq. (4.14). The code of paper, node and paper, cell is available and can be run online via COLAB [18] (code link).
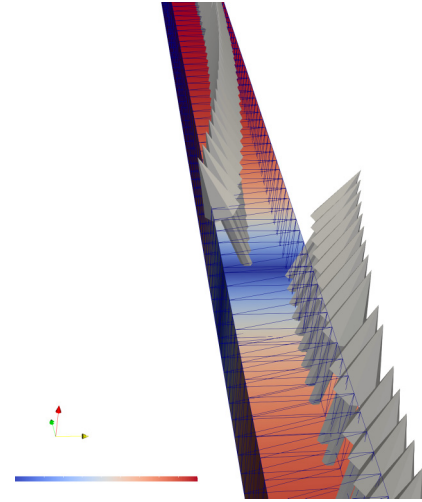

FIG. 10. MAGNUM.FE solution for $h_x = 3.9$ and $\Delta z = 0.5$ nm. For this field value where the MUMAX solution for $\Delta z = 2.0$ nm, the magnetization already points everywhere in the $M_z = 1$ direction.

field where the curvature of the $M_x(H_x)$ loop is largest. Hence, it describes the position of the kink of the $M_x(H_x)$ loop.

The (paper, node) implementation shows a good convergence toward to the analytic solution. Since we show in Appendix D that the (paper, node) implementation is equivalent to a 1D finite-element implementation the similar behavior to the three-dimensional 3D finite-element code MAGNUM.FE is not surprising.

Interestingly the MUMAX result, which is equivalent to the OOMMF result shows that the analytic solution is only obtained for infinitely small mesh sizes. For a discretization length of 2 nm, which is already a fine mesh size for common micromagnetic simulations, a significant error is obtained. The exchange length which is usually the criterion for the required discretization length amounts to $l_{\text{ex}} = \sqrt{A/K_1} = 10$ nm in this example. Hence, the discretization length of 2 nm is five times smaller than the exchange length but still leads to an error in the saturation field of more than 20% in standard FD codes. It is worth noting that this error also occurs for small magnetization inhomogeneities formed as shown in Fig. 10.

This large error is reduced successfully for the proposed first order and even better for the second order cell-based finite-difference codes. It is important to note that in this proposed implementation, the first term on the right-hand side of Eq. (4.3) has to be considered, which contains $\boldsymbol{m}_1(0)$ and $\boldsymbol{m}_2(0)$ in the Robin boundary condition.

VI. CONCLUSION

In this paper we investigate different implementations of RKKY interaction in finite-difference micromagnetic codes. The code is available and can be run online via the link in Ref. [18] and is used in the latest release of our finite-difference code MAGNUM.NP [19]. While all codes deliver reliable results for the case that the RKKY coupling acts between thin ferromagnetic layers, significant errors occur if partial domain walls are formed in the coupled ferromagnetic

layers. Partial domain walls are commonly formed in ferrimagnetic materials that are coupled antiferromagnetically to ferromagnetic layers such as in the systems of Ref. [5]. Finite-element codes show good convergence to the correct solutions. Similarly, nodal-based finite-difference codes can properly describe these antiferromagnetically coupled thick layers. If cell-based finite-difference codes are used, the most commonly used codes exhibit significant errors. The reason is that the boundary condition due to RKKY interaction is not imposed at the surface of the magnet, where it has to be imposed, but on the cell center of the finite-difference cell at the boundary. We show by using first and second order interpolation how the boundary condition can be correctly imposed at the surface of the domain. The second order cell-based scheme gives similar results as the first order nodal-based scheme.

APPENDIX A: VARIATION OF THE TOTAL ENERGY TO OBTAIN THE EQUILIBRIUM MIROMAGNETIC EQUATION

In order to obtain the equilibrium equation for the magnetization at the surface and volume of the magnet we calculate the variation of the total energy E_{tot} given by Eq. (2.5) under the constraint that the norm of the magnetization is

$$|\mathbf{m}_i| = 1. \tag{A1}$$

The constraint of the magnetization is included in the variation of the total energy by introducing Lagrange multipliers λ_1 and λ_2 within the volumes and $\lambda_{s,1}$ and $\lambda_{s,2}$ at the surfaces. The energy functional with the Lagrange multipliers is

$$\tilde{E}_{\text{tot}}(\mathbf{m}_1, \mathbf{m}_2, \lambda_1, \lambda_{s,1}, \lambda_2, \lambda_{s,2},)$$

$$= E_{\text{tot}}(\mathbf{m}_1, \mathbf{m}_2) + \int_{\Omega_2} \lambda_1 \big(1 - m_{x,1}^2 - m_{y,1}^2 - m_{z,1}^2\big) dV$$

$$+ \int_{\partial\Omega 1} \lambda_{s,1} \big(1 - m_{x,1}^2 - m_{y,1}^2 - m_{z,1}^2\big) dA$$

$$+ \int_{\Omega_2} \lambda_2 \big(1 - m_{x,2}^2 - m_{y,2}^2 - m_{z,2}^2\big) dV$$

$$+ \int_{\partial\Omega 1} \lambda_{s,2} \big(1 - m_{x,2}^2 - m_{y,2}^2 - m_{z,2}^2\big) dA. \tag{A2}$$

Here, the magnetization vector within the volume Ω_1 (accordingly for Ω_2) is

$$\mathbf{m}_1 = \begin{pmatrix} m_{x,1} \\ m_{y,1} \\ m_{z,1} \end{pmatrix}. \tag{A3}$$

For the variation of the x component of the normalized magnetization $\boldsymbol{m}_1$ we get

$$\tilde{E}_{\text{tot}}(m_{x,1} + \delta m_{x,1}, m_{y,1}, m_{z,1}, \mathbf{m}_2, \lambda_1, \lambda_{s,1}, \lambda_2, \lambda_{s,2})$$

$$= E_{\text{tot}}(m_{x,1} + \delta m_{x,1}, m_{y,1}, m_{z,1}, \mathbf{m}_2) - \int_{\Omega_1} 2\lambda_1 m_{x,1}\delta m_{x,1} dV$$

$$- \int_{\partial\Omega_1} 2\lambda_{s,1} m_{x,1}\delta m_{x,1} dA + \text{ nonlinear terms in } \delta m_{x,1}. \tag{A4}$$

For the variation of the term $E_{\text{tot}}(m_{x,1} + \delta m_{x,1}, m_{y,1}, \mathbf{m}_2)$ we get for the terms containing $\delta m_{x,1}$ from the exchange energy

$$E_{\text{ex}} = \int_{\Omega} A_{x,1}[(\tilde{}\nabla m_{x,1} + \nabla\delta m_{x,1})(\tilde{}\nabla m_{x,1} + \nabla\delta m_{x,1})\tilde{}] dV$$

$$= \int_{\Omega_1} A_{x,1}[(\nabla m_{x,1})^2 + 2\nabla m_{x,1}\nabla\delta m_{x,1} + (\nabla\delta m_{x,1})^2\tilde{}] dV. \tag{A5}$$

Applying Green's first identity to transform the term $2\nabla m_{x,1}\nabla\delta m_{x,1}$ to a linear term in $\delta m_{x,1}$ and keeping only the linear terms in $\delta m_{x,1}$ we obtain

$$E_{\text{ex}} = -\int_{\Omega_1} 2\nabla \cdot (A_{x,1}\nabla m_{x,1})\delta m_{x,1} dV$$

$$+ \int_{\partial\Omega_1} A_{x,1}[2\nabla m_{x,1}\delta m_{x,1}]\mathbf{n} dA. \tag{A6}$$

For the totaI energy we consider here all terms that lead to surface contributions, which are the exchange energy and the RKKY interaction. If we consider only the linear terms in $\delta m_{x,1}$ we obtain

$$\tilde{E}_{\text{tot}}(m_{x,1} + \delta m_{x,1}, m_{y,1}, m_{z,1}, \mathbf{m}_2, \lambda_1, \lambda_{s,1}, \lambda_2, \lambda_{s,2})$$

$$= -\int_{\Omega_1} 2\nabla \cdot (A_{x,1}\nabla m_{x,1})\delta m_{x,1} dV$$

$$+ \int_{\partial\Omega_1} A_{x,1}[2\nabla m_{x,1}\delta m_{x,1}]\mathbf{n} dA$$

$$- \int_{\partial\Omega_1\cap\partial\Omega_2} J_{\text{rkky}}\delta m_{x,1} m_{2,x} dA - \int_{\Omega_1} 2\lambda_1 m_{x,1}\delta m_{x,1} dV$$

$$- \int_{\partial\Omega_1} 2\lambda_{s,1} m_{x,1}\delta m_{x,1} dA. \tag{A7}$$

From Eq. (A7) we get within the volume Ω_1 of the magnet

$$-2\lambda_1 m_{x,1} - 2\nabla \cdot (A_{x,1}\nabla m_{x,1}) = 0, \tag{A8}$$

$$-2\lambda_1 m_{y,1} - 2\nabla \cdot (A_{y,1}\nabla m_{y,1}) = 0, \tag{A9}$$

$$-2\lambda_1 m_{z,1} - 2\nabla \cdot (A_{z,1}\nabla m_{z,1}) = 0, \tag{A10}$$

$$m_{x,1}^2 + m_{y,1}^2 + m_{z,1}^2 = 1.$$

Equations (A8)–(A10) can be written in the form

$$\mathbf{m}_1 \times 2\nabla \cdot (\mathbf{A}_1 \nabla\mathbf{m}_1) = 0, \tag{A11}$$

where

$$\mathbf{A}_1 = \begin{pmatrix} A_{x,1} & 0 & 0 \\ 0 & A_{y,1} & 0 \\ 0 & 0 & A_{z,1} \end{pmatrix}. \tag{A12}$$

The other energy contributing terms that do not contain derivates in the energy are trivially included and only lead to contributions to the volume equilibrium condition. One obtains for the volume Ω_i,

$$\mathbf{m}_i \times [2\nabla \cdot (\mathbf{A}_i \nabla \mathbf{m}_i) + J_{s,i}\mathbf{H}_{\text{ext}} + 2K_{1,i}(\mathbf{m}_i \cdot \mathbf{k}_i)\mathbf{k}_i] = 0, \tag{A13}$$

Which is convenient to write as

$$\mathbf{m}_i \times \underbrace{\left[\frac{2\nabla \cdot (\mathbf{A}_i \nabla \mathbf{m}_i)}{J_{s,i}} + \mathbf{H}_{\text{ext}} + \frac{2K_{1,i}}{J_{s,i}}(\mathbf{m}_i \cdot \mathbf{k}_i)\mathbf{k}_i \right]}_{\mathbf{H}_{\text{eff}}} = 0. \tag{A14}$$

1. Surface

From Eq. (A7) we get on the surface of the magnet $\partial\Omega_1$,

$$E_{\text{tot}} = \int_{\partial\Omega_1} A_{1,x}[2\nabla m_{x,1}\delta m_{x,1}\ ]\mathbf{n}dA$$
$$- \int_{\partial\Omega_1 \cap \partial\Omega_2} J_{\text{rkky}}\delta m_{x,1}m_{x,2}dA - \int_{\partial\Omega_1} 2\lambda_{s,1}m_{x,1}\delta m_{x,1}dA. \tag{A15}$$

Hence, we get the following boundary condition at $\partial\Omega_1 \cap \partial\Omega_2$:

$$2\mathbf{A}_1(\nabla\mathbf{m}_1)\mathbf{n} - J_{\text{rkky}}\mathbf{m}_2 = -2\lambda_{s,1}\mathbf{m}_1, \tag{A16}$$

which leads to

$$\mathbf{m}_1 \times [2\mathbf{A}_1(\nabla\mathbf{m}_1)\mathbf{n} - J_{\text{rkky}}\mathbf{m}_2] = 0, \tag{A17}$$

and for the boundary $\partial\Omega_1 \backslash (\partial\Omega_1 \cap \partial\Omega_2)$, we get

$$\mathbf{m}_1 \times [2\mathbf{A}_1(\nabla\mathbf{m}_1)\mathbf{n}] = 0. \tag{A18}$$

We can rewrite (A18) by building the cross product with $\mathbf{m}_1$:

$$\mathbf{m}_1 \times [\mathbf{m}_1 \times [2\mathbf{A}_1(\nabla\mathbf{m}_1)\mathbf{n} - J_{\text{rkky}}\mathbf{m}_2]] = 0, \tag{A19}$$

$$\underbrace{\left[\underbrace{2\mathbf{A}_1\mathbf{m}_1(\nabla\mathbf{m}_1)\mathbf{n}}_{\mathbf{nA}_1\nabla \underbrace{\mathbf{m}_1^2}_{1}} \right] \mathbf{m}_1}_{0} - \underbrace{(\mathbf{m}_1\mathbf{m}_1)}_{1} 2\mathbf{A}_1(\nabla\mathbf{m}_1)\mathbf{n}$$
$$- J_{\text{rkky}}(\mathbf{m}_1 \cdot \mathbf{m}_2)\mathbf{m}_1 + \underbrace{(\mathbf{m}_1\mathbf{m}_1)}_{1} J_{\text{rkky}}\mathbf{m}_2$$
$$= 0. \tag{A20}$$

Hence, one obtains the following Robin boundary conditions at the common surface $\partial\Omega_1 \cap \partial\Omega_2$:

$$2\mathbf{A}_1(\nabla\mathbf{m}_1)\mathbf{n} = -J_{\text{rkky}}(\mathbf{m}_1 \cdot \mathbf{m}_2)\mathbf{m}_1 + J_{\text{rkky}}\mathbf{m}_2. \tag{A21}$$

The same calculation can be applied for the second region described my $\boldsymbol{m}_2$.

APPENDIX B: DERIVATION OF ANALYTIC SOLUTION OF RKKY COUPLED 1D WIRE

In order to obtain the analytical solution for the 1D wire of Sec. III (Fig. 1) we start from the effective field within the volume and use, for the magnetization, Eq. (3.6).

$$\mathbf{H}_{\text{eff}} = \frac{2A}{J_s} \begin{pmatrix} \frac{\partial^2}{\partial^2 z}\cos[\varphi(z)] \\ \frac{\partial^2}{\partial^2 z}\sin[\varphi(z)] \\ 0 \end{pmatrix} + \begin{pmatrix} H_x \\ 0 \\ 0 \end{pmatrix} + \frac{2K_1}{J_s} \begin{pmatrix} 0 \\ \sin[\varphi(z)] \\ 0 \end{pmatrix}. \tag{B1}$$

Using the notation $\varphi = \varphi(z)$ and using the equilibrium condition

$$\mathbf{m} \times \mathbf{H}_{\text{eff}} = \begin{pmatrix} \cos(\varphi) \\ \sin(\varphi) \\ 0 \end{pmatrix} \times \mathbf{H}_{\text{eff}} = 0, \tag{B2}$$

we see that all components of Eq. (B2) are zero except the z component for which we obtain

$$\frac{2A}{J_s}\frac{\partial^2\varphi}{\partial^2 z} - H_x\sin(\varphi) + \frac{K_1}{J_s}\sin(2\varphi) = 0. \tag{B3}$$

We multiply Eq. (B3) with $\frac{\partial\varphi}{\partial z}$ and obtain

$$\frac{2A}{J_s}\underbrace{\frac{\partial^2\varphi}{\partial^2 z}\frac{\partial\varphi}{\partial z}}_{\frac{1}{2}\frac{\partial}{\partial z}\left[\frac{\partial\varphi}{\partial z}\right]^2} - H_x\underbrace{\sin(\varphi)\frac{\partial\varphi}{\partial z}}_{-\frac{\partial\cos(\varphi)}{\partial\varphi}} + \frac{K_1}{J_s}\underbrace{\sin(2\varphi)\frac{\partial\varphi}{\partial z}}_{-\frac{1}{2}\frac{\partial\cos(2\varphi)}{\partial\varphi}} = 0. \tag{B4}$$

We integrate Eq. (B4) from $-\infty$ to z,

$$\int_{-\infty}^{z} \frac{A}{J_s}\frac{\partial}{\partial z}\left[\frac{\partial\varphi}{\partial z}\right]^2 + H_x\frac{\partial\cos(\varphi)}{\partial z} - \frac{K_1}{2J_s}\frac{\partial\cos(2\varphi)}{\partial z}dz = 0, \tag{B5}$$

and obtain

$$\frac{A}{J_s}\left(\frac{\partial\varphi(z)}{\partial z}\right)^2 - \frac{A}{J_s}\underbrace{\left(\frac{\partial\varphi(-\infty)}{\partial z}\right)^2}_{0}$$
$$+ H_x\cos[\varphi(z)] - H_x\cos[\varphi(-\infty)]$$
$$- \frac{K_1}{2J_s}\cos[2\varphi(z)] + \frac{K_1}{2J_s}\cos[2\varphi(-\infty)]$$
$$= 0. \tag{B6}$$

For fields $H_x \gg \frac{2K_1}{J_s}$ it follows that $\varphi(-\infty) = 0$. Hence, we obtain the following differential equation:

$$\frac{A}{J_s}\left(\frac{\partial\varphi}{\partial z}\right)^2 + H_x\cos[\varphi(z)] - H_x - \frac{K_1}{2J_s}\cos[2\varphi(z)] + \frac{K_1}{2J_s}$$
$$= 0. \tag{B7}$$

In order to solve Eq. (B7) we have to take care of the boundary condition according to Eq. (A17). Due to symmetry we obtain an odd function of the angle $\varphi(z)$ [Eq. (3.7)], which is equivalent to

$$\begin{aligned} m_{x,1} &= m_{x,2}, \\ m_{y,1} &= -m_{y,2}. \end{aligned} \tag{B8}$$

Hence, we obtain for the general boundary condition at $z = 0$,

$$
\begin{pmatrix} \cos\varphi \\ \sin\varphi \\ 0 \end{pmatrix} \times \left[2A \begin{pmatrix} \frac{\partial}{\partial z}\cos\varphi \\ \frac{\partial}{\partial z}\sin\varphi \\ 0 \end{pmatrix} - J_{\text{rkky}} \begin{pmatrix} \cos\varphi \\ -\sin\varphi \\ 0 \end{pmatrix} \right] = 0,
$$
(B9)

which leads to

$$
2A\frac{\partial\varphi}{\partial z} = -J_{\text{rkky}}\sin(2\varphi).
$$
(B10)

We multiply Eq. (B7) with A and evaluate it at the position $z = -0$, of the interface, where we can insert Eq. (B10):

$$
\underbrace{\left(A\frac{\partial\varphi}{\partial z}\right)^2}_{-\frac{1}{2}J_{\text{rkky}}\sin(2\varphi_0)} + AH_xJ_s\cos(\varphi_0) - AH_xJ_s
$$
$$
- \frac{AK_1J_s}{2J_s}\cos(2\varphi_0) + \frac{AK_1J_s}{2J_s}
$$
$$
= 0.
$$
(B11)

Hence in the limit of $H_x > \frac{2K_1}{J_s}$ we obtain this closed form for the angle φ_0:

$$
\left[\frac{1}{2}J_{\text{rkky}}\sin(2\varphi_0)\right]^2 + AH_xJ_s\cos(\varphi_0) - AH_xJ_s
$$
$$
- \frac{AK_1}{2}\cos(2\varphi_0) + \frac{AK_1}{2}
$$
$$
= 0.
$$
(B12)

Using $H_x = h_x\frac{2K_1}{J_s}$ one obtains

$$
\frac{J_{\text{rkky}}^2}{4AK_1}\sin^2(2\varphi_0) + 2h_x\cos(\varphi_0) - 2h_x - \frac{1}{2}\cos(2\varphi_0) + \frac{1}{2} = 0.
$$
(B13)

We express for a given angle φ_0 the corresponding field h_x,

$$
H_x = \frac{2K_1}{J_s}h_x = \frac{2K_1}{J_s}\frac{1}{4}\frac{\cos(2\varphi_0) - 1 - \overbrace{\frac{J_{\text{rkky}}^2}{2AK_1}}^{j_{\text{red}}}\sin^2(2\varphi_0)}{\cos(\varphi_0) - 1},
$$
(B14)

where we have introduced the dimensionless coupling parameter,

$$
j_{\text{red}} = \frac{J_{\text{rkky}}^2}{2AK_1}.
$$
(B15)

The angle at the interface φ_0 as function of the external field H_x for different values of j_{red} that is obtained from the numerical solution of Eq. (B14) is shown in Fig. 3.

For sufficiently strong h_x the angle at the interface is exactly $\varphi_0 = 0$. If we start from this large field and decrease the field the critical field is reached if this angle starts to deviate from zero, that is, if $\varphi_0 > 0$ in Eq. (B14). Calculating the limit yields, for the nucleation field of

the domain,

$$
H_{x,\text{sat}} = \frac{2K_1}{J_s}h_{x,\text{sat}}
$$
$$
= \frac{2K_1}{J_s}\lim_{\varphi_0\to 0}\frac{1}{4}\frac{\cos(2\varphi_0) - 1 - \frac{J_{\text{rkky}}^2}{2AK_1}\sin^2(2\varphi_0)}{\cos(\varphi_0) - 1}
$$
$$
= \frac{2K_1}{J_s}\left(1 + \frac{J_{\text{rkky}}^2}{AK_1}\right).
$$
(B16)

The field $h_{x,\text{sat}}$ can also be interpreted as the saturation field. After calculating the angle φ_0 for a particular field h_x, also the entire domain wall profile $\varphi(z)$ can be obtained. For the sake of an analytical solution, not $\varphi(z)$ but $z(\varphi)$ is calculated. From Eq. (B7) it follows that

$$
\frac{\partial z}{\partial\varphi} = \pm\sqrt{\frac{1}{-\frac{J_sH_x}{A}\cos[\varphi(z)] + \frac{J_sH_x}{A} + \frac{K_1}{2A}\cos[2\varphi(z)] - \frac{K_1}{2A}}}.
$$
(B17)

The indefinite integral of Eq. (B17) is

$$
\tilde{z}(\varphi) = \int\frac{\partial z}{\partial\varphi}d\varphi
$$
$$
= \sqrt{\frac{K_1\cos(\varphi) + K_1 - H_{\text{ext}}J_s}{(K_1 - H_{\text{ext}}J_s/2)[H_{\text{ext}}J_s - K_1\cos(\varphi) - K_1]}}
$$
$$
\times \frac{\sin(\varphi/2)}{|\sin(\varphi/2)|}\sqrt{A}\tanh^{-1}
$$
$$
\times \left[\cos(\varphi/2)\sqrt{\frac{2K_1 - H_{\text{ext}}J_s}{K_1\cos(\varphi) + K_1 - H_{\text{ext}}J_s}}\right].
$$
(B18)

Hence, the relation between the angle φ and the position z is given by

$$
z(\varphi) = \int_{\varphi_0}^{\varphi}\frac{\partial z}{\partial\varphi}d\varphi = \tilde{z}(\varphi) - \tilde{z}(\varphi_0).
$$
(B19)

APPENDIX C: DERIVATION OF FINITE-DIFFERENCE EXPRESSIONS FOR A JUMP OF THE EXCHANGE CONSTANT AT MATERIAL INTERFACES

In the following we will derive expressions for the exchange field at material interfaces. We start from the general expression for the exchange field that is given according to Eq. (A14) by

$$
\mathbf{H}_{\text{ex}} = \frac{2}{J_s(\mathbf{x})}\nabla\cdot[A(\mathbf{x})\nabla\mathbf{m}].
$$
(C1)

In the following we assume that in Ω_1 and Ω_2 different magnetic materials with different exchange constants are present, as shown in Fig. 1. Within each region the exchange constant is assumed to be constant. Hence, within Ω_1 the following holds:

$$
\mathbf{H}_{\text{ex},1} = \frac{2}{J_s(\mathbf{x})}\nabla\cdot[A(\mathbf{x})\nabla\mathbf{m}] = \frac{2A_1}{J_{s,1}}\Delta\mathbf{m}.
$$
(C2)

In order to solve this problem for the entire domain, we split the finite-difference solution into two parts. In the following we consider a 1D problem, where the magnetization only
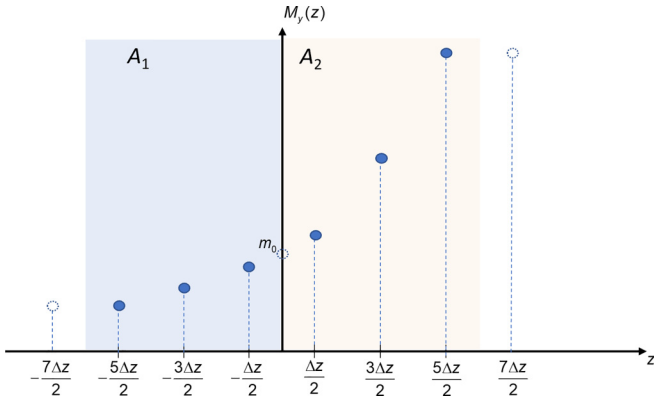
FIG. 11. Cell-based finite-difference discretization when at the interface at $z = 0$ the exchange constant exhibits a jump.

varies along the z axis (e.g., a situation as shown in Fig. 3). Equation (C2) simplifies to

$$\mathbf{H}_{\text{ex},1}(z) = \frac{2A_1}{J_{s,1}}\mathbf{m}''_1(z). \qquad (C3)$$

For all discretization points that are not located at the boundary of the region a standard three-point stencil can be used for the evaluation of the second derivative $\mathbf{m}''_1(z)$.

The discretization point where the interface between the two magnets comes into play is at $z = -\Delta z/2$, which we discuss in the following. To evaluate

$$\mathbf{H}_{\text{ex}}\left(-\frac{\Delta z}{2}\right) = \frac{2A_1}{J_{s,1}}\mathbf{m}''_1\left(-\frac{\Delta z}{2}\right) \qquad (C4)$$

we approximate the second derivative by the derivative of the first derivative,

$$\mathbf{m}''_1\left(-\frac{\Delta z}{2}\right) \approx \frac{\mathbf{m}'_1(0) - \mathbf{m}'_1(-\Delta z)}{\Delta z}. \qquad (C5)$$

The first derivative with the domain at $z = -\Delta z$ can be simply approximate:

$$\mathbf{m}'_1(-\Delta z) \approx \frac{\mathbf{m}_1\left(-\frac{\Delta z}{2}\right) - \mathbf{m}_1\left(-\frac{3\Delta z}{2}\right)}{\Delta z}. \qquad (C6)$$

In order to calculate $\mathbf{m}'_1(0)$ at the interface, we introduce the unknown ghost point $\mathbf{m}_0 = \mathbf{m}_1(0)$ and write

$$\mathbf{m}'_1(0) \approx \frac{\mathbf{m}_0 - \mathbf{m}_1\left(-\frac{\Delta z}{2}\right)}{\Delta z/2}. \qquad (C7)$$

1. Jump in the exchange constant A—cell-based FD

All commonly used finite-difference codes use a cell-based approach [6–8,21]. Special care has to be taken if jumps in the material parameters within the computed domain occur [9]. In the following we assume that the material parameter A jumps at $z = 0$ as shown in Fig. 11. Hence the magnetization is not differentiable at $z = 0$. According to Eq. (2.9) the normal derivative of the magnetization shows a jump of

$$2A_1(\boldsymbol{\nabla}\mathbf{m}_1)\mathbf{n} = 2A_2(\boldsymbol{\nabla}\mathbf{m}_2)\mathbf{n}, \qquad (C8)$$

since

$$\mathbf{m}_0 := \mathbf{m}_1(0) = \mathbf{m}_2(0), \qquad (C9)$$

where $\mathbf{m}_0$ denotes the magnetization at the boundary between the two materials.

We introduce the variable

$$\begin{aligned} \mathbf{m}(z) &= \mathbf{m}_1(z) \quad \text{for} \;\; z \leqslant 0, \\ \mathbf{m}(z) &= \mathbf{m}_2(z) \quad \text{for} \;\; z \geqslant 0. \end{aligned} \qquad (C10)$$

With Eqs. (C8) and (C9) we can calculate the unknown $\mathbf{m}_1(0)$ and $\mathbf{m}_2(0)$. From Eq. (C8) it follows for the x component that

$$A_1 \frac{\mathbf{m}_0 - \mathbf{m}\left(-\frac{\Delta z}{2}\right)}{\Delta z/2} = A_2 \frac{\mathbf{m}\left(\frac{\Delta z}{2}\right) - \mathbf{m}_0}{\Delta z/2}. \qquad (C11)$$

From Eq. (C11) $\mathbf{m}_0$ can be calculated:

$$\mathbf{m}_0 = \frac{A_2\mathbf{m}\left(\frac{\Delta z}{2}\right) + A_1\mathbf{m}\left(-\frac{\Delta z}{2}\right)}{A_1 + A_2}. \qquad (C12)$$

Substituting $\mathbf{m}_0$ into Eqs. (C7) and (C4) and neglecting all terms linear in $\mathbf{m}(-\Delta z/2)$, one obtains

$$\mathbf{H}_{\text{ex}}\left(-\frac{\Delta z}{2}\right) = \frac{2A_1}{J_{s,1}\Delta z^2}\left[\frac{2A_1\mathbf{m}(-3\Delta z/2)}{A_1 + A_1} + \frac{2A_2\mathbf{m}(\Delta z/2)}{A_1 + A_2}\right]. \qquad (C13)$$

Neglecting terms parallel to $\mathbf{m}(-\Delta z/2)$ in the effective field is justified by the fact that they do not change the dynamics of the Landau-Lifshitz-Gilbert equation at $\frac{d}{dt}\mathbf{m}(-\Delta z/2)$. This can be simply understood since the right-hand side of the Landau-Lifshitz-Gilbert only contains terms $\mathbf{m}(-\Delta z/2) \times \mathbf{H}_{\text{eff}}$. Any contribution of $\mathbf{H}_{\text{eff}} \propto \mathbf{m}(-\Delta z/2)$ cancels, since $\mathbf{m}(-\Delta z/2) \times \mathbf{m}(-\Delta z/2) = 0$.

It is worth noting that Eq. (C13) can be used everywhere in space. If in some region $A := A_1 = A_2$ it reduces to the well known equation for the exchange field [12]:

$$\mathbf{H}_{\text{ex}}\left(k\frac{\Delta z}{2}\right) = \frac{2A}{J_s\Delta z^2}\{\mathbf{m}[(k-1)\Delta z/2] + \mathbf{m}[(k+1)\Delta z/2]\}. \qquad (C14)$$

APPENDIX D: EQUIVALENCE OF 1D FINITE-ELEMENT CODE AND NODAL-BASED FINITE-DIFFERENCE CODE

In contrast to finite-difference methods, where the derivatives are approximated with finite differences, finite-element methods use the basis function to interpolate the unknown function at the domain. The domain is represented with finite elements. The micromagnetic effective field $\boldsymbol{H}_{\text{eff}}$ can be calculated from the total energy E_{tot} by

$$-\int_\Omega J_s\mathbf{H}_{\text{eff}} \cdot \mathbf{v}dV = \delta E_{\text{tot}}(\mathbf{m}, \mathbf{v}), \qquad (D1)$$

where the functions $\mathbf{v}$ are test functions that are 1 on the finite-element node and zero at all other finite-element nodes. Linear or higher order test functions can be used. The right-hand side of Eq. (D1) is the Gâteaux derivative of the total energy $E_{\text{tot}}(\mathbf{m})$ in the direction $\mathbf{v}$, which can be calculated by finite-element packages such as FENICS [22]. The integration

over the test functions allows one to write Eq. (D1) in a discrete form, using the magnetization $\boldsymbol{m}_j$ at nodes points j, as

$$\mathbf{A}_{ij}\mathbf{H}_{\text{eff},j} = \mathbf{F}_{ij}\mathbf{m}_j. \tag{D2}$$

Calculation of the effective field according to Eq. (D2) would require the solution of a linear system of equations. Hence, mass lumping can be used to approximate the matrix $\mathbf{A}_{ij}$ with a diagonal form $\tilde{\mathbf{A}}_{ij} = a_{ii}\delta_{ij} \approx \mathbf{A}_{ij}$, that can be sim-

ply inverted,

$$\mathbf{H}_{\text{eff},j} \approx \tilde{\mathbf{A}}^{-1}\mathbf{F}_{ij}\mathbf{m}_j. \tag{D3}$$

Equation (D1) shows that the total energy entirely determines the effective field. In the following we will show that the bulk exchange term of Eq. (D3) for a spacer layer (Ω_s) is equivalent to a surface energy of the form of Eq. (D6) with proper scaling of the exchange constant.

The bulk exchange is given by

$$E_{\text{ex}}(\mathbf{m}) = \int_{\Omega_s} \left(\begin{array}{l} A_x\left[\left(\frac{\partial m_x}{\partial x}\right)^2 + \left(\frac{\partial m_y}{\partial x}\right)^2 + \left(\frac{\partial m_z}{\partial x}\right)^2\right] + A_y\left[\left(\frac{\partial m_x}{\partial y}\right)^2 + \left(\frac{\partial m_y}{\partial y}\right)^2 + \left(\frac{\partial m_z}{\partial y}\right)^2\right] \\ +A_z\left[\left(\frac{\partial m_x}{\partial z}\right)^2 + \left(\frac{\partial m_y}{\partial z}\right)^2 + \left(\frac{\partial m_z}{\partial z}\right)^2\right] \end{array} \right) dV. \tag{D4}$$

Without loss of generality we assume that the spacer layer is parallel to the $x - y$ plane. Hence, we set $A_x = 0$, $A_y = 0$, and assume no volume nodes in the spacer region. Since we assume a linear basis function for the discretization of $\boldsymbol{m}$, the gradient of $\boldsymbol{m}$ is constant within each finite element. Hence, we can replace the integral in the z direction just by Δz. From Eq. (D4) we obtain

$$E_{\text{ex}}(\mathbf{m}) = E_{\text{ex}}(\mathbf{m}_1, \mathbf{m}_2)$$
$$= \int_{V_{\text{spacer}}} \frac{A_z}{\Delta z^2}[(m_{x,2} - m_{x,1})^2$$
$$+ (m_{y,2} - m_{y,1})^2 + (m_{z,2} - m_{z,1})^2] \underbrace{\Delta z dA}_{dV}, \tag{D5}$$

where $\boldsymbol{m}_1$ is the magnetization as a function of space on one side of the spacer and $\boldsymbol{m}_2$ on the opposing side (Fig. 12). We aim to set the exchange parameters A_x, A_y, and A_z in a way to reach

$$E_{\text{ex}}(\mathbf{m}_1, \mathbf{m}_2) = E_{\text{rkky}}(\mathbf{m}_1, \mathbf{m}_2) = -\int J_{\text{rkky}}\mathbf{m}_1 \cdot \mathbf{m}_2 dA. \tag{D6}$$

Considering

$$m_{x,i}^2 + m_{y,i}^2 + m_{z,i}^2 = 1 \tag{D7}$$

leads to

$$E_{\text{ex}}(\mathbf{m}) = \int_F \frac{A_z}{\Delta z}[2 - 2\mathbf{m}_1 \cdot \mathbf{m}_2]dA, \tag{D8}$$

where F is the area of the space layer to the magnet on one side.

Rescaling the energy leads to

$$E'_{\text{ex}}(\mathbf{m}) = -\int_F \underbrace{\frac{2A_z}{\Delta z}}_{J_{\text{rkky}}} \mathbf{m}_1 \cdot \mathbf{m}_2 dA. \tag{D9}$$

Comparing (D6) and (D9) leads to

$$J_{\text{rkky}} = \frac{2A_z}{\Delta z}, \tag{D10}$$

$$A_z = \frac{J_{\text{rkky}}\Delta z}{2}. \tag{D11}$$

In the following we use the bulk exchange of the spacer layer and the derived condition, Eq. (D11), in order to calculate the effective field at the node points of the spacer layer. This discretization of the effective field at the interface is compared with the nodal-based finite-difference method.

In order to simplify the notation, we introduce

$$m_{x,i-1} = m_x(-3\Delta z/2),$$
$$m_{x,i} = m_x(-\Delta z/2),$$
$$m_{x,i+1} = m_x(\Delta z/2). \tag{D12}$$

Since linear basis functions are used, the gradient within the finite elements is constant. Hence, one can write for the
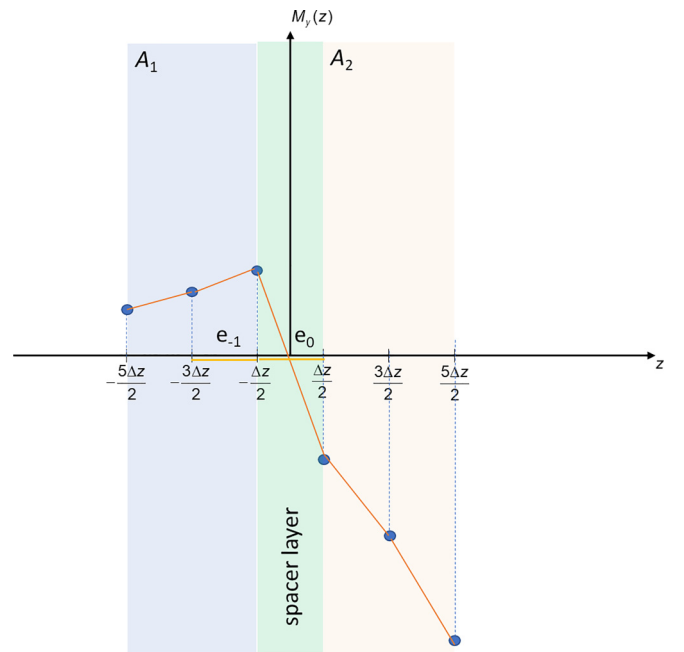

FIG. 12. Finite-element representation of RKKY coupling using a spacer layer with properly chosen exchange constants. Here two finite elements are shown: element e_{-1} and element e_0. Within the elements the magnetization is linearly interpolated (orange line).

total energy of all terms including the magnetization $m_{x,i}$,

$$
\begin{aligned}
E_{\text{ex}} = {} & F \int_{e_{-1}} \frac{A_1}{\Delta z^2} [(m_{x,i} - m_{x,i-1})^2 \\
& + (m_{y,i} - m_{y,i-1})^2 + (m_{z,i} - m_{z,i-1})^2] dz \\
& + F \int_{e_0} \frac{A_{\text{rkky}}}{\Delta z^2} [(m_{x,i+1} - m_{x,i})^2 \\
& + (m_{y,i+1} - m_{y,i})^2 + (m_{z,i+1} - m_{z,i})^2] dz + \cdots ,
\end{aligned}
$$
(D13)

where F is the interface area between spacer and the magnet (in the x and y directions). Here, we only include the energies of the element e_{-1} and element e_0 since we only want to derive the effective field at the nodal point, $m_{x,i} = m_x(-\Delta z/2)$.

The mass lumped equation for the effective field according to Eq. (D3) can be written in the form of the Box scheme [23] with the corresponding volume $V_i = F\Delta z$ for each nodal point i as

$$
\begin{aligned}
H_{\text{ex},x}(-\Delta z/2) & = -\frac{1}{V_i J_{s,\text{average}}} \frac{\partial E_{\text{ex}}}{\partial m_{x,i}} = -\frac{1}{F J_s \Delta z/2} \frac{\partial E_{\text{ex}}}{\partial m_{x,i}} \\
& = -\frac{1}{J_s \Delta z/2} \frac{\partial}{\partial m_{x,i}} \left\{ \frac{A_{\text{rkky}}}{\Delta z} [(m_{x,i+1} - m_{x,i})^2 \right.
\end{aligned}
$$

$$
\begin{aligned}
& \left. \quad + (m_{y,i+1} - m_{y,i})^2 + (m_{z,i+1} - m_{z,i})^2] \right\} \\
& - \frac{1}{J_s \Delta z/2} \frac{\partial}{\partial m_{x,i}} \left\{ \frac{A_1}{\Delta z} [(m_{x,i} - m_{x,i-1})^2 \right. \\
& \left. \quad + (m_{y,i} - m_{y,i-1})^2 + (m_{z,i} - m_{z,i-1})^2] \right\},
\end{aligned}
$$
(D14)

since the saturation magnetization in the spacer layer is zero $J_{s,\text{average}} = J_s/2$. For the exchange field one gets

$$
\begin{aligned}
H_{\text{ex},x}(-\Delta z/2) & = -\frac{1}{F J_s \Delta z/2} \frac{\partial E_{\text{ex}}}{\partial m_{x,i}} \\
& = \frac{2}{J_s \Delta z^2} (2 A_{\text{rkky}} m_{x,i+1} + 2 A_1 m_{x,i-1}).
\end{aligned}
$$
(D15)

Using the proper value of A_{rkky} to represent J_{rkky} according to Eq. (D11) one gets

$$
\mathbf{H}_{\text{ex}}(-\Delta z/2) = \frac{2}{J_s \Delta z^2} (J_{\text{rkky}} \Delta z \mathbf{m}_{i+1} + 2 A_1 \mathbf{m}_{i-1}),
$$
(D16)

which is equivalent to the derived equation for the nodal finite-difference formula according to Eq. (4.22)

---

[1] W. Maloney, Sputtered multilayer films for digital magnetic recording, IEEE Trans. Magn. **15**, 1135 (1979).

[2] L. A. Francis and K. Poletkin, *Magnetic Sensors and Devices: Technologies and Applications* (CRC Press, Boca Raton, FL, 2017).

[3] S. S. P. Parkin, Systematic Variation of the Strength and Oscillation Period of Indirect Magnetic Exchange Coupling through the 3*d*, 4*d*, and 5*d* Transition Metals, Phys. Rev. Lett. **67**, 3598 (1991).

[4] S. S. P. Parkin, N. More, and K. P. Roche, Oscillations in Exchange Coupling and Magnetoresistance in Metallic Superlattice Structures: Co/Ru, Co/Cr, and Fe/Cr, Phys. Rev. Lett. **64**, 2304 (1990).

[5] M. Heigl, C. Vogler, A.-O. Mandru, X. Zhao, H. J. Hug, D. Suess, and M. Albrecht, Microscopic origin of magnetization reversal in nanoscale exchange-coupled ferri/ferromagnetic bilayers: Implications for high energy density permanent magnets and spintronic devices, ACS Appl. Nano Mater. **3**, 9218 (2020).

[6] A. Vansteenkiste and B. Van de Wiele, MUMAX: A new high-performance micromagnetic simulation tool, J. Magn. Magn. Mater. **323**, 2585 (2011).

[7] M. J. Donahue and M. J. Donahue, *OOMMF User's Guide, Version 1.0* (U.S. Department of Commerce, National Institute of Standards and Technology, Gaithersburg, ND, 1999).

[8] M.-A. Bisotti, D. Cortés-Ortuño, R. Pepper, W. Wang, M. Beg, T. Kluyver, and H. Fangohr, FIDIMAG—A finite difference atomistic and micromagnetic simulation package, J. Open Res. Software **6**, 22 (2018).

[9] P. Heistracher, C. Abert, F. Bruckner, T. Schrefl, and D. Suess, Proposal for a micromagnetic standard problem: Domain wall pinning at phase boundaries, J. Magn. Magn. Mater. **548**, 168875 (2022).

[10] D. Suess, V. Tsiantos, T. Schrefl, J. Fidler, W. Scholz, H. Forster, R. Dittrich, and J. J. Miles, Time resolved micromagnetics using a preconditioned time integration method, J. Magn. Magn. Mater. **248**, 298 (2002).

[11] Y. Toga, M. Nishino, S. Miyashita, T. Miyake, and A. Sakuma, Anisotropy of exchange stiffness based on atomic-scale magnetic properties in the rare-earth permanent magnet $Nd_2Fe_{14}B$, Phys. Rev. B **98**, 054418 (2018).

[12] J. E. Miltat and M. J. Donahue, Numerical micromagnetics: Finite difference methods, in *Handbook of Magnetism and Advanced Magnetic Materials*, edited by H. Kronmüller and S. Parkin (John Wiley & Sons, Ltd, New York, 2007).

[13] Y. Pinchover and J. Rubinstein, *An Introduction to Partial Differential Equations* (Cambridge University Press, Cambridge, UK, 2005).

[14] H. Kronmüller and D. Goll, Micromagnetic theory of the pinning of domain walls at phase boundaries, Phys. B (Amsterdam) **319**, 122 (2002).

[15] H. J. Waring, Y. Li, C. Moutafis, I. J. Vera-Marun, and T. Thomson, Magnetization dynamics in synthetic ferromagnetic thin films, Phys. Rev. B **104**, 014419 (2021).

[16] S. M. Dunn, A. Constantinides, and P. V. Moghe, Finite difference methods, interpolation and integration, in *Numerical Methods in Biomedical Engineering*, edited by S. M. Dunn, A. Constantinides, and P. V. Moghe (Academic Press, Burlington, MA, 2006), Chap. 6, pp. 163–208.

[17] S. S. Rao, *Finite Difference Methods, in Encyclopedia of Vibration*, edited by S. Braun (Elsevier, Oxford, 2001), pp. 520–530.

[18] RKKY code used for the paper: (online) https://colab.research.google.com/drive/1Luj-1csvHeC7y0LY9Q9UHSgm2azMfkjF?usp=sharing, (n.d.).

[19] F. Bruckner, S. Koraltan, C. Abert, and D. Suess, MAGNUM.NP—A PYTORCH based GPU enhanced finite difference micromagnetic simulation framework for high level development and inverse design, arXiv:2302.08843.

[20] C. Abert, L. Exl, F. Bruckner, A. Drews, and D. Suess, MAGNUM.FE: A micromagnetic finite-element simulation code based on FENICS, J. Magn. Magn. Mater. **345**, 29 (2013).

[21] P. Heistracher, F. Bruckner, C. Abert, C. Vogler, and D. Suess, Hybrid FFT algorithm for fast demagnetization field calculations on non-equidistant magnetic layers, J. Magn. Magn. Mater. **503**, 166592 (2020).

[22] The FENICS Book, https://fenicsproject.org/book/.

[23] C. W. Gardiner, *Handbook of Stochastic Methods* (Springer, Berlin, 1985), Vol. 3.